Nonlinear integrated guidance and control based on adaptive backstepping scheme

Seyed Hamed Seyedipour and Mohsen Fathi Jegarkandi
Department of Aerospace Engineering, Sharif University of Technology, Tehran, Iran, and
Saeed Shamaghdari
Department of Electrical Engineering, Iran University of Science and Technology, Tehran, Iran

Abstract

Purpose – The purpose of this paper is to design an adaptive nonlinear controller for a nonlinear system of integrated guidance and control.

Design/methodology/approach – A nonlinear integrated guidance and control approach is applied to a homing, tail-controlled air vehicle. Adaptive backstepping controller technique is used to deal with the problem, and the Lyapanov theory is used in the stability analysis of the nonlinear system. A nonlinear model of normal force coefficient is obtained from an existing nonlinear model of lift coefficient which was validated by open loop response. The simulation was performed in the pitch plane to prove the benefits of the proposed scheme; however, it can be readily extended to all the three axes.

Findings – Monte Carlo simulations indicate that using nonlinear adaptive backstepping formulation meaningfully improves the performance of the system, while it ensures stability of a nonlinear system.

Practical implications – The proposed method could be used to obtain better performance of hit to kill accuracy without the expense of control effort.

Originality/value – A nonlinear adaptive backstepping controller for nonlinear aerodynamic air vehicle is designed and guaranteed to be stable which is a novel-based approach to the integrated guidance and control. This method makes noticeable performance improvement, and it can be used with hit to kill accuracy.

Keywords Stability, Nonlinear control, Adaptive backstepping, Air vehicle, Integrated guidance and control

Paper type Research paper

Introduction

Conventional guidance and control design approach of air vehicles treats guidance and control as two distinct sub-systems. Typically, guidance algorithm (acts as outer loop) generates acceleration command based on the relative target-interceptor position change, while the control algorithm (acts as inner loop) makes use of interceptor states to track commanded acceleration. In the conventional guidance and control design methodology, it is common to design each of the two sub-systems separately which is followed by integrating them. In case of unsatisfactory results, modifications are subsequently made to each unit to improve the overall system performance. This approach usually leads to numerous design iterations and does not exploit the synergistic coupling between guidance and control. In addition to the above lines, in traditional design approach, changes in relative geometry is considered to be much slower than that in the air vehicle dynamic. However, in the homing phase, because of rapid changes in relative geometry, this assumption is not valid, and it can clearly lead to degraded performance. As Palumbo *et al.* (2004) discussed, the problem arises when the interception of highly maneuverable targets, including ballistic and cruise targets, is needed.

To improve the performance of guidance and control system, integrated guidance and control (IGC) design methodology was established which eliminates design iterations and takes more advantages of synergistic coupling between guidance and control. This design approach uses both guidance and control states to directly generate fin deflection command in one loop. The benefits of the IGC concept are well reported and compared with the conventional design approach in relevant works (Menon and Ohlmeyer, 2001; Palumbo *et al.*, 2004). Various control methods are applied to the IGC approach to address this design problem. Some of them are listed as follows: Menon and Ohlmeyer (2001) applied feedback linearization method to IGC, Sharma and Richards (2004) used backstepping and neural networks based on the zero effort miss (ZEM) concept. Xin *et al.* (2006) applied $\theta - D$ method to IGC problem. Mingzhe and Guangren (2008) and Yiyin *et al.* (2010) designed IGC against ground-fixed targets and ground-moving targets, respectively. Shima *et al.* (2006) used the sliding mode control based on the ZEM.

More recent, Zhurbal and Idan (2011) studied the estimation effect on the performance of IGC system, Yan and

The current issue and full text archive of this journal is available on Emerald Insight at: **www.emeraldinsight.com/1748-8842.htm**

Aircraft Engineering and Aerospace Technology: An International Journal
89/3 (2017) 415–424

[DOI 10.1108/AEAT-12-2014-0209]

The authors would like to thank Tavakkolie Farhad for his valuable comments on developing model and simulating the methods.

Received 6 December 2014
Revised 26 January 2016
Accepted 5 February 2016

Ji (2012) designed IGC for dual control missile and Yan *et al.* (2013) used backstepping and input to state the stability method to IGC problem.

So far, multitude of IGC systems were designed with backstepping controller in relevant works (Sharma and Richards, 2004; Yan *et al.*, 2013). However, they all use the linear aerodynamic model which can lead to degraded performance in realistic scenarios, including large initial heading error (HE) and high angle of attack flight. In contrast, recent studies (Fathi *et al.*, 2009a, 2009b; Shamaghdari and Nikravesh, 2012; Shamaghdari *et al.*, 2014) have shown that using nonlinear aerodynamic model will lead to different results. Therefore, a new approach to the IGC, that is nonlinear aerodynamic model with backstepping controller, is proposed in this paper.

An IGC system with the nonlinear aerodynamic model is presented in the next section. Section 3 presents model dynamic validation. Section 4 includes adaptive controller design. Numerical results are shown in Section 5, and finally, concluding remarks are presented in the last section.

Problem formulation

This section presents an IGC system for pitch channel of a skid to turn roll stabilized tail-controlled air vehicle. As mentioned in the previous section, IGC system is used in the homing phase and does not have a noticeable effect on other flight phases. Thus, the end game phase is considered in this paper. The distance between air vehicle and target, the line of sight angle (LOS), velocity, flight path angle and acceleration are, respectively, denoted by R, λ, V, γ and a. Figure 1 shows the planar engagement geometry, where $X_I-O_I-Z_I$ is a Cartesian inertial reference frame.

The kinematic equations can be written as follows:

$$\dot{\gamma}_{AV,T} = \frac{a_{AV,T}}{V_{AV,T}} \tag{1}$$

$$\dot{R} = -V_{AV}\cos(\gamma_{AV} - \lambda) - V_T\cos(\gamma_T + \lambda) \tag{2}$$

$$\dot{\lambda} = \frac{V_\lambda}{R} = \frac{1}{R}[V_T \sin(\gamma_T + \lambda) - V_{AV}\sin(\gamma_{AV} - \lambda)] \tag{3}$$

where air vehicle and target are, respectively, denoted by AV and T subscripts. In addition, $\dot{R}$ and $\dot{\lambda}$ denote closing velocity and LOS rate, respectively. Assuming constant velocity for both vehicles during engagement and using equations (1), (2) and (3), one can write:

$$\ddot{\lambda} = \frac{-2\dot{R}}{R}\dot{\lambda} + \frac{a_T}{R}\cos(\gamma_T + \lambda) - \frac{a_{AV}}{R}\cos(\gamma_{AV} - \lambda) \tag{4}$$

It should be noted that no estimation of target acceleration has been assumed. The linear aerodynamic model approximates air vehicle acceleration by $L_\alpha\alpha$ with constant L_α, where α denotes angle of attack. However, in case of using nonlinear aerodynamic model, acceleration can be written as $q_\infty SC_N/m$, where q, S_{ref} and m are dynamic pressure, air vehicle aerodynamic reference area and air vehicle mass, respectively. C_N is normal force coefficient which is usually assumed to vary with angle of attack. However, this assumption cannot be used in all flight conditions.

A nonlinear lift coefficient model (C_L) was issued by Reichert (1992) and has been used in several works (Nichols *et al.*, 1993; Mracek and Cloutier, 1997; Bennani *et al.*, 1998). Introducing pitch damping derivative (c_{m_q}), the model was reinforced by Mracek and Cloutier (1997), which was later used by Xin and Balakrishnan (2003 and 2008). Bennani *et al.* (1998) assumed that the vehicle flies at small angles of attack. Thus, C_N will be approximately equal to C_L. However, for an air vehicle which flies at a high angle of attack, this assumption is not valid. There is an alternative method for obtaining nonlinear normal force coefficient, multiplying the C_L values by cos (α) to obtain C_N data numerically, which is called Mracek–Cloutier model in the rest of this paper. Assuming symmetric air vehicle, it is enough to consider the positive angles of attack. Then, the least squares method could be used to obtain the nonlinear C_N equation. The resultant equation is a polynomial of the third degree or higher. This work uses third degree polynomial which has the following form:

$$C_N = a_1\alpha^3 + a_2\alpha^2 + a_3\alpha \tag{5}$$

In addition, linear fit which is used later is given by the following equation:

$$\text{Linear fit: } = \frac{\partial C_N}{\partial \alpha}|_{\alpha=0}\,\alpha = a_3\alpha \tag{6}$$

One can differentiate to obtain the following equation:

$$\frac{dC_N}{dt} = C_N\dot{\alpha},\ C_{N_\alpha} = 3a_1\alpha^2 + 2a_2\alpha + a_3 \tag{7}$$

where:

$$\dot{\alpha} = \dot{q} - \frac{q_\infty S_{ref}}{mV_{AV}}C_N \tag{8}$$

where q is the air vehicle pitch rate. Moreover, the pitch moment can be written as:

$$\dot{q} = \frac{M(\alpha, q, \delta e)}{I_{yy}} = \frac{q_\infty S_{ref} L_{ref}}{I_{yy}}c_m(\alpha, q, \delta e) \tag{9}$$

where δe, L_{ref}, I_{yy} and $c_m(\alpha, q, \delta e)$ are elevator deflection angle, reference length, moment of inertia and total aerodynamic

Figure 1 Planar engagement geometry

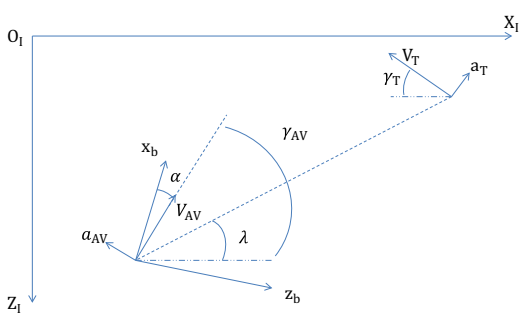

moment coefficient about pitch axis, respectively. Aerodynamic pitching moment coefficient is assumed to have the following form:

$$c_m(\alpha, q, \delta e) = c_{m_\alpha}(\alpha) + c_{m_q} q + c_{m_{\delta e}} \delta e \tag{10}$$

where c_{m_q} and $c_{m_{\delta e}}$ are constant factors and $c_{m_\alpha}(\alpha)$ is a nonlinear function with respect to angle of attack. Assuming small deviation from collision course for both air vehicle and target during homing phase and taking $\mathbf{X}^T = [\dot{\lambda} \quad C_N \quad q]$ as a state vector, IGC system can be written as:

$$\begin{cases} \dot{x}_1 = a_{11}x_1 + a_{12}x_2 + \Delta_1 \quad \text{I} \\ \dot{x}_2 = C_{N_\alpha}\dot{\alpha} + \Delta_2, \dot{\alpha} = (x_3 + a_{22}x_2) \quad \text{II} \\ \dot{x}_3 = c\left[c_{m_\alpha}(\alpha) + c_{mq}\, q + bu\right] + \Delta_3 \quad \text{III} \end{cases} \tag{11}$$

where $a_{11} = -2\dot{R}/R$, $a_{12} = -L_{C_N}/R$, $L_{C_N} = q_\infty S_{ref}/mR$, $a_{22} = -q_\infty S_{ref}/mV_{AV}$, $b = c_{m_{\delta e}}$ and $c = q_\infty S_{ref} L_{ref}/I_{yy}$ are parameters, while $u = \delta e$ is controller input. In addition, Δ_i is bounded uncertainties which satisfy the following equation:

$$|\Delta_i| \leq \rho_i \tag{12}$$

where ρ_i is the upper band of uncertainty for each state in equation (11). It should be noted that R, V_{AV} and q_∞ are considered to be constant during the homing phase; however, they are varying in simulation.

A good interception and consequently small miss distance (the least interceptor-target distance) lie in settling the LOS rate to zero, while the most important control objective of an interceptor is internal stability of the whole system dynamic. Afterward, the angle of attack and pitch rate should also be kept in certain limits. Moreover, control effort (time integral of absolute elevator deflection) is an important performance index for a variety of problems. As a result, small miss distance and control effort as well as internal stability of the system dynamic are considered to be the control objectives in this work.

Air vehicle dynamics validation

To validate the developed aerodynamic model, open loop step response to step input is considered for the angle of attack and pitch rate. It should be noted that the air vehicle used in this work has unstable open loop response when the whole system states (LOS rate, normal force coefficient and pitch rate) are considered. In contrast, ignoring the first state (LOS rate) which is always an unstable dynamic, one can see the tendency of angle of attack and pitch rate toward a trim value when the step elevator is applied to the Mracek–Cloutier model. Figures 2 and 3 show the open loop response of angle of attack and pitch rate to step elevator input.

Figures 2 and 3 illustrate the inability of the linear fit to describe nonlinearities of Mracek–Cloutier model, while the third degree polynomial does it well. Figure 4 shows a DC gain of angle of attack which is the steady state response to various elevator inputs.

Figure 4 demonstrates that linear fit behaves linearly while third degree polynomial tracks Mracek–Cloutier model perfectly. As a result, the third degree polynomial can be used in the controller design to describe the Mracek–Cloutier model.

Figure 2 Open loop step response of angle of attack

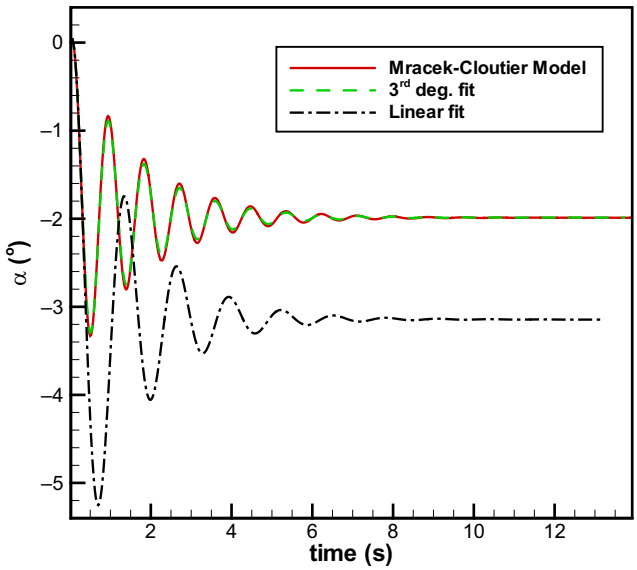

Figure 3 Open loop step response of pitch rate

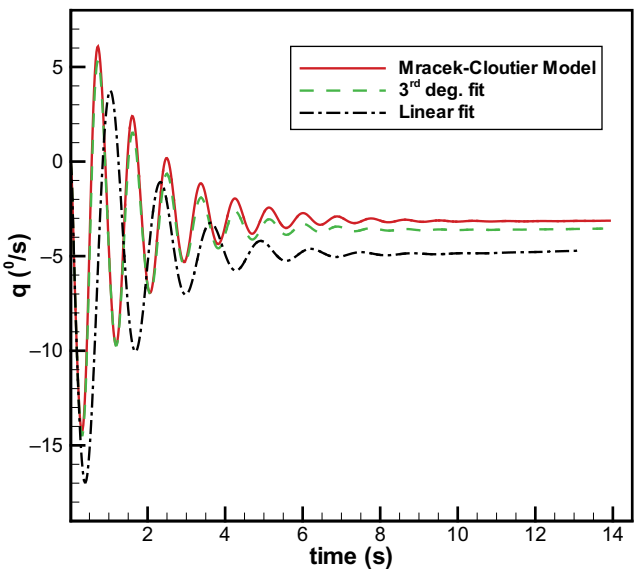

Integrated guidance and control controller design and stability analysis

This section presents controller design based on the Lyapunov theory and backstepping controller. The obtained adaptive IGC law nullifies LOS rate while simultaneously ensuring the stability of the system of equation (11).

The design procedure is started by taking $s_1 = x_1$ as the first tracking error. Thus, one can define the first Lyapunov function candidate as follows:

$$V_1 = \frac{1}{2}s_1^2 + \frac{1}{2\lambda_1}\tilde{\rho}_1^2 \tag{13}$$

Figure 4 Angle of attack DC gain

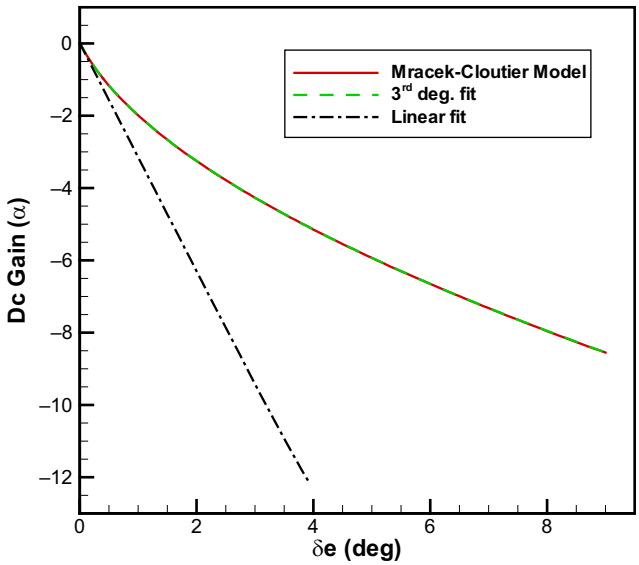

where λ_1 is a design parameter, $\tilde{\rho}_1 = \rho_1 - \hat{\rho}_1$ and $\hat{\rho}_1$ is an estimated value for ρ_1. Differentiating V_1 yields:

$$\dot{V}_1 = s_1[a_{11}x_1 + a_{12}x_2 + \Delta_1] + \frac{1}{\Delta_1}\tilde{\rho}_1\dot{\tilde{\rho}}_1 \tag{14}$$

taking:

$$x_{2_C} = -\frac{1}{a_{12}}[a_{11}x_1 + k_1 s_1 + \hat{\rho}_1 s_1],\ k_1 > 0 \tag{15}$$

As a virtual control and $\dot{\hat{\rho}}_1 = \lambda_1(s_1^2 - \sigma_1\hat{\rho}_1)$ as an update law, equation (14) can be rewritten as:

$$\dot{V}_1 \le -k_1 s_1^2 - \hat{\rho}_1 s_1^2 + \rho_1 s - \tilde{\rho}_1(s_1^2 + \sigma_1(-\hat{\rho}_1 \pm \rho_1)) \tag{16}$$

where σ_1 is a design parameter. Direct computation yields:

$$\dot{V}_1 \le -k_1 s_1^2 - \rho_1 s_1^2 + \rho_1 s_1 - \sigma_1\tilde{\rho}_1^2 + \sigma_1\tilde{\rho}_1\rho_1 \tag{17}$$

Equation (17) can be rewritten as:

$$\dot{V}_1 \le -k_1 s_1^2 - \rho_1 s_1^2 + \rho_1 s_1 - \sigma_1\left(\frac{\tilde{\rho}_1^2}{2} - \frac{\rho_1^2}{2}\right) \tag{18}$$

Then, we have:

$$\dot{V}_1 \le -k_1 s_1^2 - \sigma_1\left(\frac{\tilde{\rho}_1^2}{2} - \frac{\rho_1^2}{2}\right) + \frac{\rho_1}{4} \tag{19}$$

The second tracking error can be taken as $s_2 = x_2 - x_{2_C}$. So, one can define the second Lyapunov function as:

$$V_2 = \frac{1}{2}s_2^2 + \frac{1}{2\lambda_2}\tilde{\rho}_2^2 \tag{20}$$

where λ_2 is a design parameter, $\tilde{\rho}_2 = \rho_2 - \hat{\rho}_2$ and $\hat{\rho}_2$ is an estimated value for ρ_2. Differentiating equation (20) yields:

$$\dot{V}_2 = s_2\left[C_{N_\alpha}\dot{\alpha} + \Delta_2 - \dot{x}_{2_C}\right] + \frac{1}{\lambda_2}\tilde{\rho}_2\dot{\tilde{\rho}}_2 \tag{21}$$

where we have $\dot{x}_{2_C} = -[(a_{11} + k_1 + \hat{\rho}_1)\dot{s}_1 + \dot{\hat{\rho}}_1 s_1]/a_{12}$. Using $\dot{\hat{\rho}}_2 = \lambda_2(s_2^2 - \sigma_2\hat{\rho}_2)$ as an update law, where σ_2 is a design parameter and taking x_{3_C} as:

$$x_{3_C} = -\frac{1}{C_{N_\alpha}}\left[C_{N_\alpha}a_{22}x_2 + k_2 s_2 - \dot{x}_{2_C} + \hat{\rho}_2 s_2\right],\ k_2 > 0 \tag{22}$$

One can rewrite equation (21) to obtain:

$$\dot{V}_2 \le -k_2 s_2^2 - \hat{\rho}_2 s_2^2 + \rho_2 s_2 - \tilde{\rho}_2(s_2^2 + \sigma_2(-\hat{\rho}_2 \pm \rho_2)) \tag{23}$$

which has the same form as equation (16). Hence, after some straightforward calculation, it yields:

$$\dot{V}_2 \le -k_2 s_2^2 - \sigma_2\left(\frac{\tilde{\rho}_2^2}{2} - \frac{\rho_2^2}{2}\right) + \frac{\rho}{4} \tag{24}$$

Third tracking error can be taken as $s_3 = x_3 - x_{3_C}$. Therefore, one can define the third Lyapunov function as:

$$V_3 = \frac{1}{2}s_3^2 + \frac{1}{2\lambda_3}\tilde{\rho}_3^2 \tag{25}$$

where λ_3 is a design parameter, $\tilde{\rho}_3 = \rho_3 - \hat{\rho}_3$ and $\hat{\rho}_3$ is an estimated value for ρ_3. Differentiating equation (25) yields:

$$\dot{V}_3 = s_3\left[M(\alpha) + M_q q + bu + \Delta_3 - \dot{x}_{3_C}\right] + \frac{1}{\lambda_3}\tilde{\rho}_3\dot{\tilde{\rho}}_3 \tag{26}$$

where:

$$\dot{x}_{3_C} = \frac{-1}{C_{N_\alpha}}\left[a_{22}\frac{d}{dt}(C_{N_\alpha}x_2) + (k_2 + \hat{\rho}_2)\dot{s}_2 - \ddot{x}_{2_C} + \frac{dC_{N_\alpha}}{dt}x_{3_C} - \dot{\hat{\rho}}_2 s_2\right] \tag{27}$$

where:

$$\frac{d}{dt}(C_{N_\alpha}x_2) = \frac{dC_{N_\alpha}}{dt}x_2 + C_{N_\alpha}\dot{x}_2,\ \frac{dC_{N_\alpha}}{dt} = \frac{dC_{N_\alpha}}{d\alpha}\frac{d\alpha}{dt} \tag{28}$$

The term $\ddot{x}_{2_C}$ in equation (27) is as follows:

Table I Air vehicle-target engagement scenarios

Scenario no.	Scenario mode	Maneuver time (s)	Acceleration (m/s^2)
Scenario I	*a*	2	$+10\sin(\pi t/3)$
	b	2	$-10\sin(\pi t/3)$
Scenario II	*a*	2	$+20\sin(\pi t/3)$
	b	2	$-20\sin(\pi t/3)$
Scenario III	*a*	2	$+30\sin(\pi t/3)$
	b	2	$-30\sin(\pi t/3)$
Scenario IV	*a*	2	$+30\sin(\pi t/4)$
	b	2	$-30\sin(\pi t/4)$
Scenario V	*a*	4	+15
	b	4	−15

Figure 5 Tracking errors and angle of attack for the proposed method and linear integrated guidance and control method – Scenario V-a

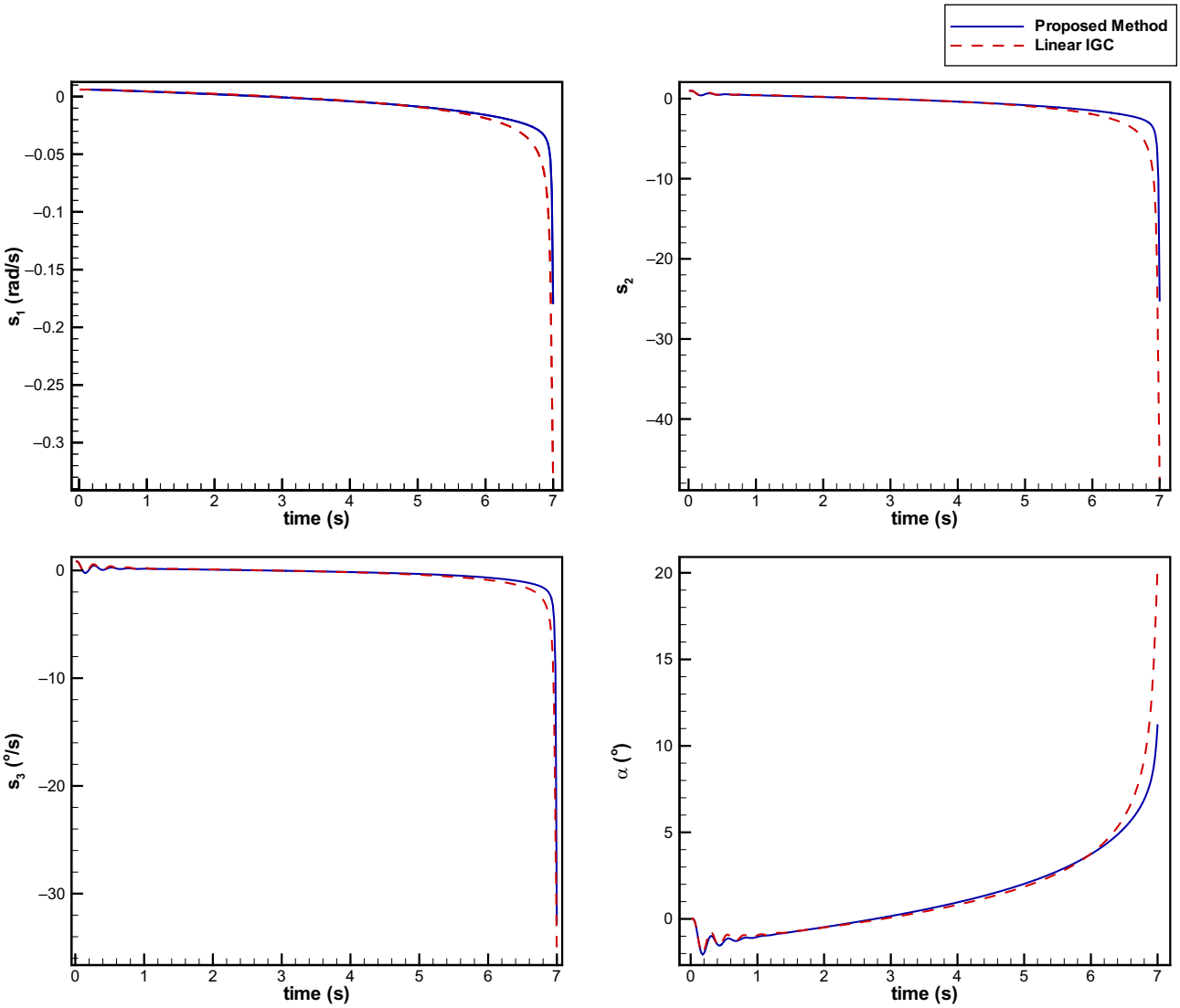

Figure 6 Elevator deflection for proposed method and linear integrated guidance and control method – Scenario V-a

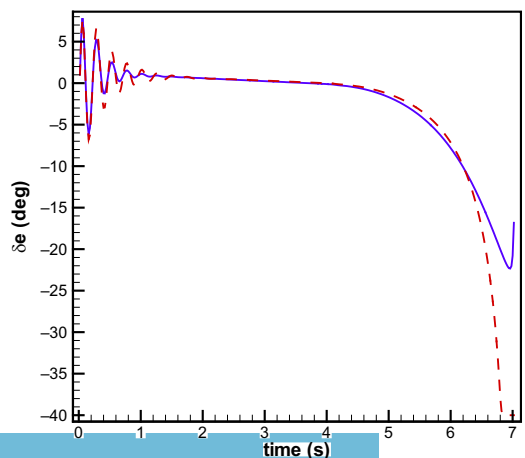

$$\ddot{x}_{2_C} = -\frac{1}{a_{12}}\left(\left[a_{11} + k_1 + \dot{\hat{\rho}}_1\right]\tilde{s}_1 + \left[2\dot{\hat{\rho}}_1 s_1 + \ddot{\hat{\rho}}_1 s_1\right]\right) \quad (29)$$

where:

$$\ddot{\hat{\rho}}_1 = \lambda_1\left(2s_1\dot{s}_1 - \sigma_1\dot{\hat{\rho}}_1\right) \quad (30)$$

The first bracket in equation (29) could be assumed to be near zero. But this assumption does not work for the second

Table II Performance of the proposed methods and linear IGC-Scenario V-a

Method	Miss distance (*m*)	Control effort (°*s*)	Peak normal acceleration (*g*)
The proposed method	0.27	33.5	13.5
Linear IGC	1.47	44.0	22.0

bracket. Concentrating on equation (26), the controller input could be defined as:

$$u = -\frac{1}{b}\left[M(\alpha) + M_q q + k_3 s_3 - \dot{x}_{3_C} + \hat{\rho}_3 s_3\right],\ k_3 > 0 \tag{31}$$

Substituting equations (27) and (31) into equation (26) yields:

$$\dot{V}_3 \le -k_3 s_3^2 - \hat{\rho}_3 s_3^2 + \rho_3 s_3 - \tilde{\rho}_3(s_3^2 + \sigma_3(-\hat{\rho}_3 \pm \rho_3)) \tag{32}$$

Equation (32) has the same form of equations (16) and (23). As a result, it can be rewritten as:

$$\dot{V}_3 \le -k_3 s_3^2 - \sigma_3\left(\frac{\tilde{\rho}_3^2}{2} - \frac{\rho_3^2}{2}\right) + \frac{\rho_3}{4} \tag{33}$$

All Lyapunov derivatives obtained as equation (19), equations (24) and (33) have the same form as the following equation:

$$\dot{V}_i \le -k_i s_i^2 - \sigma_i\frac{\tilde{\rho}_i^2}{2} + \sigma_i\frac{\rho_i^2}{2} + \frac{\rho_i}{4} \tag{34}$$

which could be rewritten as:

$$\dot{V}_i \le -2k_i V_i + \frac{\eta_i}{\lambda_i}\tilde{\rho}_i^2 + \varepsilon \tag{35}$$

where:

$$\varepsilon = +\sigma_i\frac{\rho_i^2}{2} + \frac{\rho_i}{4} \tag{36}$$

Let $k_i \ge \mu/2,\ \mu > 0$ and $\mu_i \le \lambda_i\sigma_i$, equation (35) yields:

$$\dot{V}_i \le -\mu_i V_i + \varepsilon \tag{37}$$

Assuming, $\mu \ge \varepsilon/r$, one can conclude that $\dot{V}_i$ is less or equal to zero for all $t \ge t_0$. As a result, $s_i,\ \tilde{\rho}_i,\ x_i;\ i = 1,\ 2,\ 3$ are bounded. Taking equations (15) and (22) as virtual input and equation (31) as the elevator input, the system of equation (11) is guaranteed to be stable.

It should be noted that the stability proof of linear aerodynamic model could be easily conducted with the formulation developed in this section. The only desired modifications are setting a_1 and a_2 equal to zero besides assigning appropriate value to a_3 in equation (5). The following section presents the numerical results.

Figure 7 Cumulative probability of miss distance – Scenario I

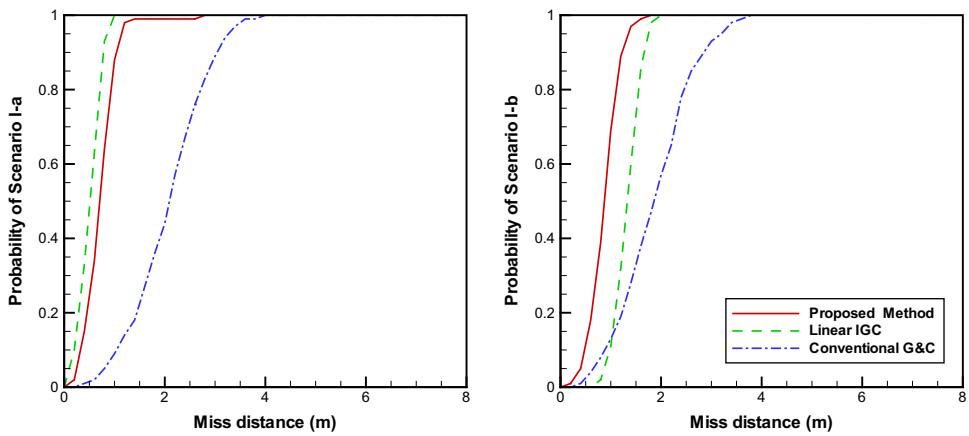

Figure 8 Cumulative probability of miss distance – Scenario II

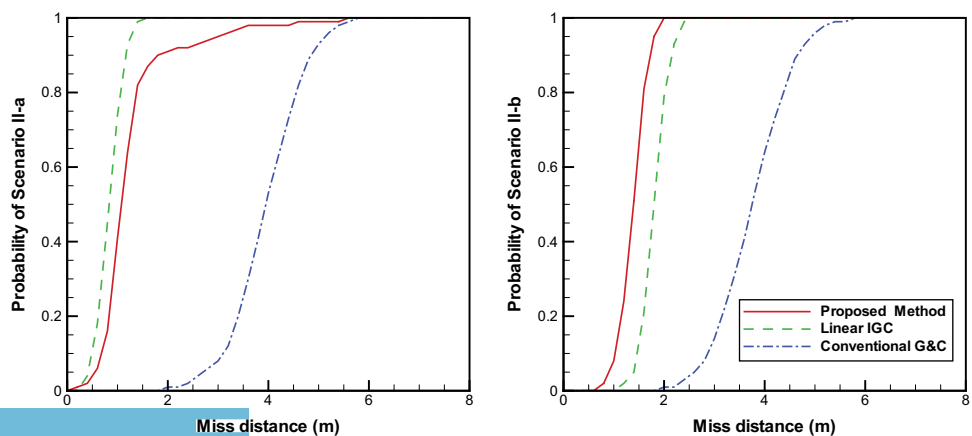

Aircraft Engineering and Aerospace Technology: An International Journal
Volume 89 · Number 3 · 2017 · 415–424

Simulation results

This section presents simulation results of three methods. The proposed method is the first one. The second one which could be achieved by simplifying the proposed method is linear aerodynamic approximation and called linear IGC in the rest of this work. This method uses linear fit of C_N as described in equation (6). The third one is the conventional guidance and control design which uses PID controller and TPN guidance algorithm with navigation constant of 4. This method is called conventional G&C in the rest of the paper.

Some head-on homing engagement scenarios have been simulated which differ by the target acceleration. The air vehicle initially travels at the velocity of 700 m/s ($M = 2.2$), while the target initially travels at the constant velocity of

Figure 9 Cumulative probability of miss distance – Scenario III

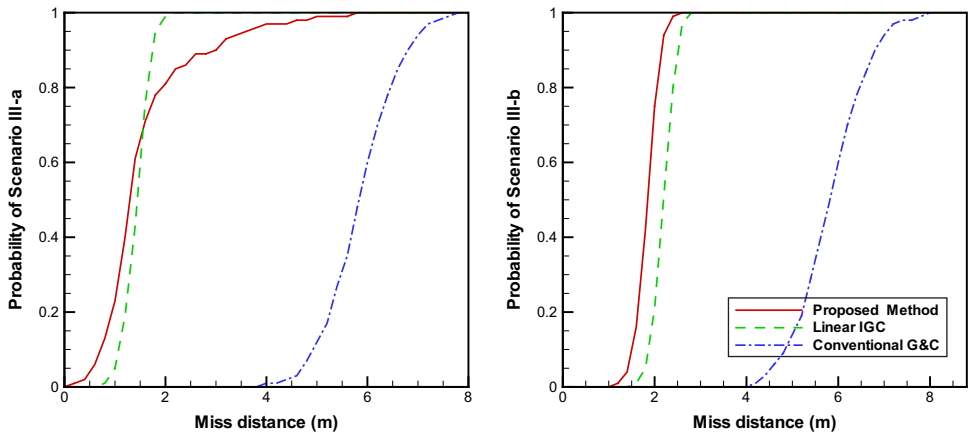

Figure 10 Cumulative probability of miss distance – Scenario IV

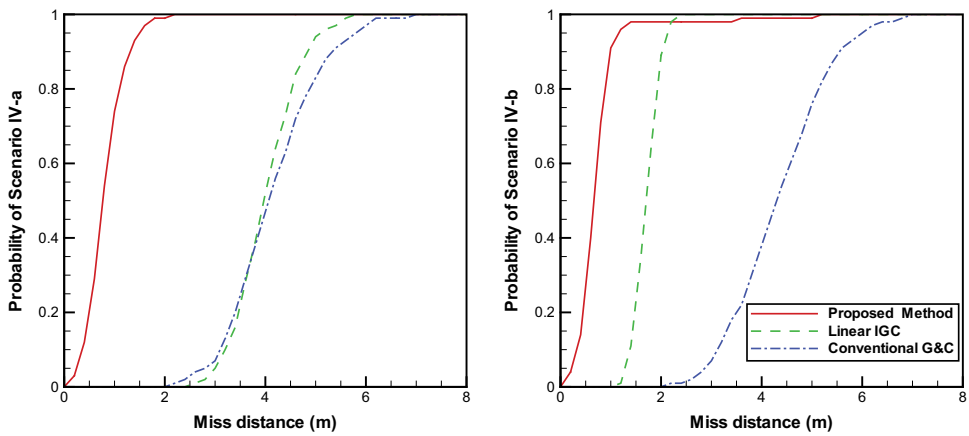

Figure 11 Cumulative probability of miss distance – Scenario V

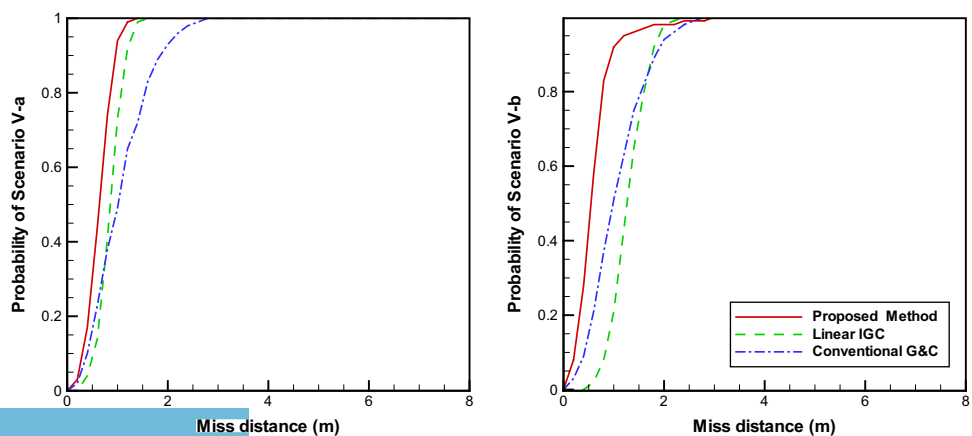

Aircraft Engineering and Aerospace Technology: An International Journal
Volume 89 · Number 3 · 2017 · 415–424

200 m/s, and then changes its acceleration in one step. Both air vehicle and target are initially flying at the same altitude of 4 km, with the initial relative range of 6 km. Range parameter which is used in the system of equation (11) and target time constant were set to $R = 500$ m and $\tau = 0.2$ s, respectively. Maximum maneuver capability of air vehicle at this altitude, maximum elevator deflection, maximum elevator deflection rate, maximum pitch rate and maximum pitch rate derivative of the air vehicle were limited to 30 g, 40°, 300°/s, 400°/s and 400°/s^2, respectively.

A high fidelity nonlinear 6 DOF simulation was used to investigate performance of the three methods. Table I presents the simulated scenarios. It should be noted that the target acceleration is directed toward its body z-axis.

Nominal run

Nominal simulation result of Scenario V-a is presented in this section. To make more realistic scenario, five degree of heading error was considered in the addition to target acceleration. Figure 5 shows three tracking error and angle of attack for both IGC methods. As second tracking error of the linear IGC is angle of attack (not normal force coefficient), it was multiplied by a factor to obtain normal force coefficient. Thus, second tracking error in Figure 5 shows normal force coefficient.

Figure 5 shows better interception performance of the proposed method in obtaining smaller LOS rate and normal force coefficient. It can be seen that as the angle of attack moves toward larger values, the performance of the linear IGC method degrades. In contrast, the proposed method performs well by fully addressing nonlinear aerodynamic characteristics of the vehicle. Figure 6 shows elevator deflection for both IGC methods.

Figure 6 shows that better interception performance of the proposed method does not come at expenses of control effort which is also clear in Table II results. Table II includes miss distance, control effort and peak normal acceleration of both methods.

Figures 5 and 6 and Table II show outstanding performance of the proposed method compared to the linear IGC method.

Monte Carlo runs

In this section, Monte Carlo results are presented to prove benefits of the proposed method. It is well-known that small miss distance is obtained as a result of nullifying LOS rate.

Table III Performance of the three methods in Monte Carlo simulations

Scenario no.	Scenario mode	Method	Miss distance (*m*)		Control effort (°*s*)		Peak normal acceleration (*g*)	
			Mean	SD	Mean	SD	Mean	SD
Scenario I	a	Proposed method	0.72	0.37	26.6	4.9	9.0	4.0
		Linear IGC	0.50	0.22	32.7	5.2	12.0	3.2
		Conventional G&C	2.07	0.75	34.1	14.5	9.6	4.5
	b	Proposed method	0.86	0.28	21.5	3.7	18.2	5.5
		Linear IGC	1.32	0.26	25.4	5.3	22.4	3.4
		Conventional G&C	1.87	0.74	34.5	15.8	8.5	4.3
Scenario II	a	Proposed method	1.25	0.78	35.5	5.9	16.9	7.6
		Linear IGC	0.83	0.25	38.5	6.0	11.5	1.0
		Conventional G&C	3.96	0.72	38.8	13.6	17.2	3.5
	b	Proposed method	1.38	0.26	21.6	3.8	25.2	3.3
		Linear IGC	1.80	0.26	21.5	4.4	24.1	3.4
		Conventional G&C	3.76	0.70	38.4	14.4	16.6	3.6
Scenario III	a	Proposed method	1.17	1.06	30.7	17.6	14.9	9.9
		Linear IGC	1.43	0.25	48.3	6.4	13.6	1.7
		Conventional G&C	5.86	0.71	44.7	12.7	21.3	1.6
	b	Proposed method	1.84	0.25	22.6	3.5	28.9	2.3
		Linear IGC	2.19	0.23	21.4	3.7	25.3	3.2
		Conventional G&C	5.82	0.76	43.2	13.3	21.4	1.6
Scenario IV	a	Proposed method	0.81	0.37	46.9	3.0	22.2	1.5
		Linear IGC	4.01	0.63	50.1	4.5	23.7	0.9
		Conventional G&C	4.14	0.90	52.3	12.9	19.6	0.4
	b	Proposed method	0.74	0.62	32.6	4.8	20.9	5.1
		Linear IGC	1.70	0.24	32.9	5.4	26.6	1.9
		Conventional G&C	4.34	0.95	54.2	12.4	19.0	0.4
Scenario V	a	Proposed method	0.64	0.24	16.0	3.5	9.5	4.7
		Linear IGC	0.85	0.25	17.2	4.1	9.6	4.4
		Conventional G&C	1.05	0.57	39.8	15.0	11.5	4.0
	b	Proposed method	0.6	0.4	39.4	4.4	17.5	5.1
		Linear IGC	1.3	0.4	53.3	6.4	22.4	1.1
		Conventional G&C	1.1	0.5	41.1	14.0	11.6	3.7

Aircraft Engineering and Aerospace Technology: An International Journal
Volume 89 · Number 3 · 2017 · 415–424

The smaller the LOS rate is, the smaller the miss distance is achieved. However, to numerically test a method in the presence of various noises and uncertainty sources, one can use Monte Carlo simulations, which are based on statistical results. The conducted Monte Carlo simulations include noise in LOS rate, acceleration and angular velocity measurements. Moreover, 10 per cent of uncertainty in aerodynamic coefficients has been assumed to examine the robustness of the proposed method. In addition, random initial heading error of $|H.E.| \leq 5°$ has been considered to make more realistic scenarios.

Figures 7 to 11 depict the cumulative probability of miss distances for each scenario. Better performance is shown by plotted curves which are farther to the left and have higher slope.

Figures 7 to 11 show that both IGC methods have better performance than conventional scheme in all scenarios. The other valuable result which is clear in Figures 7 to 11 is higher slope of the line related to the proposed method in nearly all scenarios. This feature demonstrates better performance of the proposed method when miss distance is considered as performance index. It could be seen that as the scenario becomes more stressing, the proposed method shows better performance than the others. Table III shows Monte Carlo simulation results, including mean and standard deviation (SD) of miss distance, control effort and peak normal acceleration.

Table III illustrates that as the scenario becomes more stressing, both IGC methods perform more consistently and degrade more gracefully than the conventional G&C method. In addition, it can be seen the proposed method performs more consistently than linear IGC, especially for peak normal acceleration and control effort. Furthermore, the mean miss distance of the proposed method is usually better than the two other methods, and it does not come at the expense of control effort. Table IV shows mean miss distance, control effort and peak normal acceleration improvement percentage of the proposed method in comparison to linear IGC and conventional G&C methods.

Table IV indicates that miss distance and control effort of the proposed method are better than the other two methods in most of the scenarios, and they are considerably improved in some scenarios. Moreover, mean peak normal acceleration does not increase very much.

Conclusion

The performance improvement of a new integrated guidance and control formulation versus common integrated guidance and control and conventional guidance and control method was investigated. The paper focuses on the effects of using nonlinear aerodynamics for a homing tail-controlled air vehicle. The new formulation was applied to the pitch plane with backstepping control technique. A normal force coefficient of third degree polynomial with respect to the angle of attack was selected to address nonlinearities of air vehicle aerodynamic model in controller design. The air vehicle dynamic was validated by open loop response. Validation shows that linear normal force coefficient cannot mention the nonlinear behavior of air vehicle model, while the third degree polynomial achieves model response perfectly. The novelty of this work lies in generating a full nonlinear integrated guidance and control formulation which is also proved to be stable based on the Lyapunov theory. Numerical results of high fidelity simulation show the capability of the proposed scheme to nullify the line of sight rate in the presence of noises and modeling errors. The control effort is noticeably reduced and peak normal acceleration remains in an acceptable bound.

Table IV Improvement percentage of the proposed method in Monte Carlo simulations

Scenario no.	Scenario mode	Method	Miss distance (%)	Control effort (%)	Peak normal acceleration (%)
Scenario I	a	Linear IGC	−42.5	18.7	25.0
		Conventional G&C	65.4	21.9	6.2
	b	Linear IGC	34.5	15.5	18.9
		Conventional G&C	53.9	37.8	−114.6
Scenario II	a	Linear IGC	−49.9	7.9	−46.1
		Conventional G&C	68.4	8.6	2.2
	b	Linear IGC	23.2	−0.4	−4.6
		Conventional G&C	63.2	43.8	−51.5
Scenario III	a	Linear IGC	17.7	36.5	−9.7
		Conventional G&C	80.0	31.3	30.0
	b	Linear IGC	15.9	−5.9	−14.3
		Conventional G&C	68.4	47.6	−35.2
Scenario IV	a	Linear IGC	79.7	6.4	6.5
		Conventional G&C	80.4	10.2	−13.2
	b	Linear IGC	56.8	0.8	21.4
		Conventional G&C	83.1	39.8	−9.7
Scenario V	a	Linear IGC	24.5	7.0	1.1
		Conventional G&C	39.0	59.9	17.6
	b	Linear IGC	52.5	26.0	21.9
		Conventional G&C	42.8	4.1	−51.2

References

Bennani, S., Willemsen, D.M.C. and Scherer, C.W. (1998), "Robust control of linear parametrically varying systems with bounded rates", *Journal of Guidance, Control and Dynamics*, Vol. 21 No. 6, pp. 916-922.

Fathi, J.M., Nobari, A.S., Sabzehparvar, M. and Haddadpour, H. (2009a), "Aeroelastic stability consideration of supersonic flight vehicle using nonlinear aerodynamic response surfaces", *Journal of Fluids and Structures*, Vol. 25 No. 6, pp. 1079-1101.

Fathi, J.M., Nobari, A.S., Sabzehparvar, M., Haddadpour, H. and Tavakkolie, F. (2009b), "Aeroelasticity consideration of supersonic vehicle using closed form analytical aerodynamic model", *Aircraft Engineering & Aerospace Technology*, Vol. 81 No. 2, pp. 128-136.

Menon, P.K. and Ohlmeyer, E.J. (2001), "Integrated design of agile missile guidance and autopilot systems", *Control Engineering Practice*, Vol. 9 No. 10, pp. 1095-1106.

Mingzhe, H. and Guangren, D. (2008), "Integrated guidance and control of homing missiles against ground fixed targets", *Chinese Journal of Aeronautics*, Vol. 21 No. 2, pp. 162-168.

Mracek, C.P. and Cloutier, J.R. (1997), "Full envelope missile longitudinal autopilot design using the state-dependent Riccati equation method", *Proceedings of the AIAA Guidance, Navigation, and Control Conference, New Orleans, LA*, pp. 1697-1705, available at: https://arc.aiaa.org/doi/abs/10.2514/6.1997-3767

Nichols, R., Reichert, R.T. and Rugh, W.J. (1993), "Gain scheduling for H-infinity controllers: a flight control example", *Control Systems, IEEE Transactions*, Vol. 1 No. 2, pp. 69-79.

Palumbo, N.F., Reardon, B.E. and Blauwkamp, R.A. (2004), "Integrated guidance and control for homing missile", *Johns Hopkins APL Technical Digest*, Vol. 25 No. 2, pp. 121-139.

Reichert, R.T. (1992), "Dynamic scheduling of modern robust control autopilot designs for missiles", *Control Systems, IEEE Transactions*, Vol. 12 No. 5, pp. 35-42.

Shamaghdari, S. and Nikravesh, S.K.Y. (2012), "A nonlinear stability analysis of elastic flight vehicle", *Aircraft Engineering and Aerospace Technology*, Vol. 84 No. 6, pp. 404-412.

Shamaghdari, S., Nikravesh, S.K.Y. and Haeri, M. (2014), "Integrated guidance and control of elastic flight vehicle based on robust MPC", *International Journal of Robust and Nonlinear Control*, Vol. 25 No. 15.

Sharma, M. and Richards, N.D. (2004), "Adaptive integrated guidance and control for missile interceptors", *AIAA Guidance, Navigation, and Control Conference and Exhibit, RI*.

Shima, T., Idan, M. and Golan, O.M. (2006), "Sliding-mode control for integrated missile autopilot guidance", *Journal of Guidance, Control and Dynamics*, Vol. 29 No. 2, pp. 250-260.

Xin, M. and Balakrishnan, S.N. (2003), "Missile longitudinal autopilot design using a new suboptimal nonlinear control method", *IEE Proceeding Control Theory Application*, Vol. 150 No. 6, pp. 577-584.

Xin, M. and Balakrishnan, S.N. (2008), "Nonlinear H_∞ missile longitudinal autopilot design with $\theta - D$ method", *IEEE Transactions On Aerospace And Electronic Systems*, Vol. 44 No. 1, pp. 41-56.

Xin, M., Balakrishnan, S.N. and Ohlmeyer, E.J. (2006), "Integrated guidance and control of missiles with $\theta - D$ method", *IEEE Transactions on Control Systems Technology*, Vol. 14 No. 6, pp. 981-992.

Yan, H. and Ji, H. (2012), "Integrated guidance and control for dual-control missiles based on small-gain theorem", *Automatica*, Vol. 48 No. 10, pp. 2686-2692.

Yan, H., Wang, X., Yu, B. and Ji, H. (2013), "Adaptive integrated guidance and control based on backstepping and input-to-state stability", *Asian Journal of Control*, Vol. 16 No. 1, pp. 1-7.

Yiyin, W., Mingzhe, H. and Guangren, D. (2010), "Adaptive multiple sliding surface control for integrated missile guidance and autopilot with terminal angular constraint", *Chinese Control Conference (CCC), 29th Chinese, Beijing*, pp. 2162-2166.

Zhurbal, A. and Idan, M. (2011), "Effect of estimation on the performance of an integrated missile guidance and control system", *Aerospace and Electronic Systems, IEEE Transactions*, Vol. 47 No. 4, pp. 2690-2708.

Corresponding author

Seyed Hamed Seyedipour can be contacted at: seyedipour_seyedhamed@ae.sharif.ir